Int. J. Electrochem. Sci., 10 **(2015)** 10738 - 10755

International Journal of
ELECTROCHEMICAL
SCIENCE
www.electrochemsci.org

Multifunctional "gum metal" Titanium-Based Alloy: Its Long-Term Electrochemical Behavior and Macrophage Response

S. I. Drob[1], *C. Vasilescu*[1,*], *J. M. Calderon Moreno*[1], *P. Osiceanu*[1], *P. Neacsu*[2], *A. Cimpean*[2], *D. M. Gordin*[3], *T. Gloriant*[3]

[1] Institute of Physical Chemistry "Ilie Murgulescu" of Romanian Academy, Spl. Independentei 202, 060021, Bucharest, Romania
[2] University of Bucharest, Department of Biochemistry and Molecular Biology, 91-95 Spl. Independentei, 050095 Bucharest, Romania
[3] INSA Rennes, UMR CNRS 6226 ISCR, 20 avenue des Buttes de Coësmes, 35708 Rennes cedex 7, France
[*]E-mail: cora_vasilescu@yahoo.com

Received: 28 September 2015 / *Accepted:* 27 October 2015 / *Published:* 4 November 2015

We obtained the multifunctional Ti-23Nb-0.7Ta-2Zr-1.2O alloy by the melting process with good mechanical properties, good bone tissue compatibility, superior anticorrosive resistance and negligible toxicity. In this paper we characterize this biomaterial by using both electrochemical (cyclic voltammetry and linear polarization, electrochemical impedance spectroscopy – EIS), microscopic (scanning electron microscopy – SEM) and spectroscopic (X-ray photoelectron spectroscopy – XPS) methods and macrophage-based culture studies. We analyzed its long-term behavior regarding corrosion rates, variations of the open circuit potentials and corresponding open circuit potential gradients, namely its possible susceptibility to the local corrosion, the over time evolution of the physical processes at the interface between this alloy and simulated biofluid (Ringer solution of different pH values) and also, the in time surface modifications. The alloy native passive film consists from very protective TiO_2, Nb_2O_5, ZrO_2 oxides and tantalum suboxides; it has a thickness of about 6.5 nm ± 1 nm, is more compact and thicker than that on Ti surface and is able to confer a better protection to the substrate. Long-term behavior indicated more protective passive films, higher resistance to corrosion; these passive films became more resistant in time due to new depositions from the solutions which thickened the initial passive films. SEM micrographs confirmed these new depositions having some pores. EDS elemental analysis attested the presence of calcium and phosphorous elements on the alloy surface. *In vitro* studies with RAW 264.7 macrophages performed in terms of cell survival and proliferation, morphology and pro-inflammatory mediator secretion demonstrated that the gum alloy does not sustain a persistent inflammatory response.

Keywords: titanium alloy; XPS; SEM; corrosion resistance; macrophage

1. INTRODUCTION

New generation of biomedical titanium-based alloys for long-term implantation must be free of cytotoxic elements such as vanadium, aluminum or nickel and have low elastic modulus to prevent the stress shielding effect [1-3]. Promising titanium alloys are made with beta-stabilizing and biocompatible elements such as Ta, Nb, Mo, Zr via optimization of alloy compositions and thermo-mechanical treatments [4-8]. Among these beta-type Ti-based alloys, the multifunctional Ti-23Nb-0.7Ta-2Zr-1.2O alloy composition (mol %), called "gum metal", was shown to possess "super" properties such as very high strength, low elastic modulus, high elastic recovery and high plasticity at room temperature [9-11]. These properties make this alloy an excellent candidate for various applications and particularly in the biomedical sector to replace the hard tissues of hip joints, dental roots, etc.

A good implant material must not produce adverse reactions in the surrounding tissues and must not degrade in the body biofluid; if the implant alloy contains only biocompatible elements [12,13], it satisfies the first requirement; in the same time, if its corrosion resistance is very high it accomplishes the second requirement. Another very important requirement for orthopedic implant integration is an enhanced functional activity of osteoblasts without any subsequent inflammatory reaction. Inflammation is a favorable host immune response to tissue injury or infection, but long-drawn or uncontrollable pro-inflammatory environment may lead to osteolysis and implant loosening. We have previously synthesized the Ti-23Nb-0.7Ta-2Zr-1.2O "gum metal" alloy [14] by the melting process with good mechanical properties (high strength ≈ 900 MPa; Young's modulus ≈ 60 GPa; recoverable strain ≈1.5%), superior anticorrosive resistance and negligible toxicity. This alloy exhibited excellent biocompatibility in terms of osteoblast attachment, spreading, viability, proliferation and differentiation. According to the best of our knowledge there are no other reports in literature on cellular compatibility of gum metals. In this paper we studied for the first time its long-term behavior (till 2000 immersion hours) regarding its corrosion rates, variations of the open circuit potentials and corresponding open circuit potential gradients, namely its possible susceptibility to the local corrosion, the over time evolution of the physical processes at the interface between this alloy and simulated biofluid (Ringer solution of different pH values 3.21; 7.31; 8.93) and also, the in time surface modifications. Taking into account that the potential of this material to induce unwanted immune responses has not been investigated yet, we also explored its *in vitro* effects on murine macrophage RAW 264.7 cell response. Thus, macrophage viability, morphology and activation (release of pro-inflammatory cytokines/chemokines) were assessed as compared to titanium surface. Throughout the study, we used both electrochemical (cyclic voltammetry and linear polarization, electrochemical impedance spectroscopy – EIS), microscopic (scanning electron microscopy – SEM) and spectroscopic (X-ray photoelectron spectroscopy – XPS) methods and cell culture based studies.

2. EXPERIMENTAL PART

2.1. Alloy synthesis by melting and sample preparation

As titanium, zirconium, tantalum and niobium have very different melting points and densities, the synthesis of the "gum metal" Ti-23Nb-0.7Ta-2Zr-1.2O (mol.%) alloy was realized by the cold

crucible semi-levitation melting (CCLM) technique under high vacuum, using a high-frequency magnetic induction generator heating system. With this method, the high-frequency magnetic field is used to stir the liquid, which is useful in ensuring that alloying elements are fully mixed into the melt without contamination thanks to the restricting contact points between the melt and the cold crucible. The added elements are pure solid metals, except oxygen, which was introduced through titanium oxide (TiO_2) powder. After melting, a homogenization treatment was carried out at 950°C for 16 h under high vacuum. Then, the ingot was cold rolled at room temperature to reach 1 mm in thickness that corresponds of 90% of reduction in thickness. From the shit, disc shape samples (diameter: 13 mm, thickness: 1 mm) were cut for the biological and the electrochemical tests. Then, all samples were solution treated under high vacuum at 850°C for 0.5 hour in the beta-phase field and water quenched in order to obtain a fully recrystallized beta microstructure from the cold rolled state. Finally, all samples were mechanically "mirror" polished on abrasive papers and then ultrasonically cleaned in acetone, thoroughly washed with ethanol and dried in air.

2.2. Characterization of initial surface and of film formed over time (till 2000 immersion hours)

The composition of the alloy native passive film was analyzed by X-ray photoelectron microscope; the thickness of the film was determined by the same technique. XPS equipment works at a pressure of $1.33x10^{-7}$ Pa, has a source of AlKα radiation (1486.6 eV, monocromatized) and a resolution of 0.65 eV by the full width at half maximum of Au $4f_{7/2}$ line. The thickness of the oxide existing on the alloy surface was measured by the depth profiling, layer by layer experiment using an Ar^+ ion beam with a kinetic energy of 1 keV on an area of 3 x 3 mm, an incident angle of 45^0 and spot size on the target of 100 μm.

The morphology of the surface films after various exposure periods in Ringer solution of different pH values (3.21; 7.31; 8.93) were examined by SEM technique using a FEI Quanta 3D FEG equipment at an accelerating voltage of 20 kV; elemental analysis was performed by EDS detector.

2.3. Electrochemical characterization

To simulate the real functional conditions of an implant, Ringer solutions of different pH values were used: acid pH = 3.21 can appear in case of surgery because the hydrogen concentration increases in the traumatized tissues [15]; in the case of inflammations or infections or in the distress periods of the human body, the pH can reach 9 value [16], (8.93 in our research); in the case of long-term use, the hydrolysis processes of the oxides forming the passive film could produce important local changes of pH values [17]. The composition of the Ringer solution was (g/L): NaCl – 6.8; KCl – 0.4; $CaCl_2$ – 0.2; $MgSO_4.7H_2O$ – 0.2048; $NaH_2PO_4.H_2O$ – 0.1438; $NaHCO_3$ -1.1; glucose – 1; pH = 7.31.

The over time electrochemical behavior of the studied alloy was appreciated by the cyclic voltammetry and linear polarization, and EIS methods [18-20] after certain time periods and from the monitoring of the open circuit potentials, E_{oc} and corresponding open circuit potential gradients, ΔE_{oc}. All electrode potentials referred to saturated calomel electrode – SCE. The cyclic voltammetry was

applied from about -0.8 V till +2 V with a scan rate of 1 mV/s and the following parameters were determined: corrosion, E_{corr} and passivation, E_p potentials; tendency to passivation, $|E_{corr} - E_p|$ and passive current density, i_p [21,22]. Linear polarization measurements were performed for 50 mV more negative and 50 mV more positive than E_{corr} with a scan rate of 0.1 mV/s and from Tafel representations were identified the main corrosion parameters: corrosion current density, i_{corr}; corrosion rate, V_{corr}; polarization resistance, R_p. The total quantity (ng/cm^2) of ions released into the solution was calculated using the formula [17,21,22]:

$$\text{Ion release rate} + 1.016 \cdot V_{corr} \cdot 10^5 \quad (1)$$

where V_{corr} = corrosion rate in mm/year.

The monitoring of E_{oc} comprised a period of 2000 exposure hours in Ringer solution. The open circuit potential gradients ΔE_{oc} which could appear due to the different values of the pH along the implant surface were estimated as the following differences [17,21,22]:

$$\Delta E_{oc1}(pH) = E_{oc}^{pH=3.21} - E_{oc}^{pH=7.31} \quad (2)$$

$$\Delta E_{oc2}(pH) = E_{oc}^{pH=3.21} - E_{oc}^{pH=8.93} \quad (3)$$

$$\Delta E_{oc3}(pH) = E_{oc}^{pH=7.31} - E_{oc}^{pH=8.93} \quad (4)$$

Electrochemical impedance Nyquist and Bode spectra were recorded at open circuit potential with voltage amplitude of 5 mV in a frequency range of 10^{-1} – 10^5 Hz using 7 points per decade. The electric equivalent circuit was modeled with ZVIEW program.

2.4. Cell culture

Murine macrophage RAW 264.7 cell line was purchased from American Type Culture Collection (ATCC) and grown in Dulbecco's modified Eagle's medium (DMEM) supplemented with 10% fetal bovine serum and 1% penicillin/streptomycin at 37°C in 5% CO_2 humidified air. Cells were routinely passaged using a cell scraper and for experiments they were used at passages between 10 and 20. RAW 264.7 cells were seeded onto the metallic pieces at a density of 5 x 10^4 cells·cm^{-2} for ELISA (enzyme-linked immunosorbent assay) and proliferation assays or 1.5 x 10^4 cells·cm^{-2} for cell morphology studies in two culture conditions: non-inflammatory or pro-inflammatory using 10 ng·mL^{-1} lipopolysaccharide, LPS, to induce the macrophage activation.

2.5. Macrophage proliferation assay

The ability of RAW 264.7 macrophages to adhere and proliferate on the substrates was evaluated at 24 h and 48 h post-seeding, in the presence or absence of LPS. This study was performed using a colorimetric assay, namely MTT, as previously described [23].

2.6. Fluorescence staining of actin

RAW 264.7 cells cultured onto the test materials for 24 h and 48 h, treated or non-treated with LPS, were fixed with 4 % paraformaldehyde in PBS (phosphate buffer saline) for 20 min. After rinsing with PBS, the samples with adherent cells were then permeabilized and blocked with a solution containing 0,1 % Triton X-100 and 2 % BSA (bovine serum albumin) in PBS for 1 h. In the next step the cells were subjected to fluorescence staining of the actin cytoskeleton. For this reason, RAW macrophages were rinsed again with PBS and incubated with Alexa Fluor-488 conjugated phalloidin (20 $\mu g \cdot mL^{-1}$, Life Technologies) for 20 min at room temperature, in the dark. All images were visualized with an epifluorescence inverted microscope (Olympus, IX71) and the representative fields were captured using Cell F software.

2.7. Analysis of cytokines/chemokines secretion

Quantitative determination of extracellular TNF-α (tumor necrosis factor-α), MIP-1α (macrophage inhibitory protein-1α) and RANTES (Regulated upon Activation, Normal T cell Expressed and Secreted) released in the culture medium by macrophages grown onto the metallic surfaces for 24 h and 48 h, respectively, was performed using enzyme-linked immunosorbent assay (ELISA) according to the manufacturer instructions (R&D Systems). To eliminate the variations due to difference in cell density between the samples, cytokine and chemokine secretion were normalized as previously reported [24].

2.8. Statistical analysis

The values of biological data are expressed as mean ±SD. Statistical significance was determined by one-way ANOVA test, followed by Bonferroni's multiple comparison test. A value of $p<0.05$ was considered statistically significant.

3. RESULTS AND DISCUSSION

3.1. Characterization of the initial alloy surface by XPS

XPS survey spectrum (Fig. 1) revealed the peaks for the all constituent elements of the gum alloy: Ti 2p, Nb 3d, Ta 4f, Zr 3d, and of the oxygen, O 1s [25,26]. XPS deconvoluted spectra (Fig. 2) identified the following oxides [25,26] existing on the gum alloy surface: for Ti (Fig. 2a), the very protective TiO_2 oxide and Ti_2O_3 suboxide; for Nb (Fig. 2b), very resistant Nb_2O_5 oxide; for Ta (Fig. 2c), protective tantalum suboxides; for Zr (Fig. 2d), very protective ZrO_2 oxide; also, oxygen (Fig. 2e) is present as O^{2-} ion from oxides and OH^- ion in lower quantity, probably as adsorbed ion. Thus, on gum alloy surface exists a native passive film consisting from very protective TiO_2, Nb_2O_5, ZrO_2 oxides and tantalum suboxides; this film has a thickness of about 6.5 nm ± 1 nm [27]; it is a bigger thickness than that of the native passive film on Ti surface of about 1.5 nm – 5.4 nm [28].

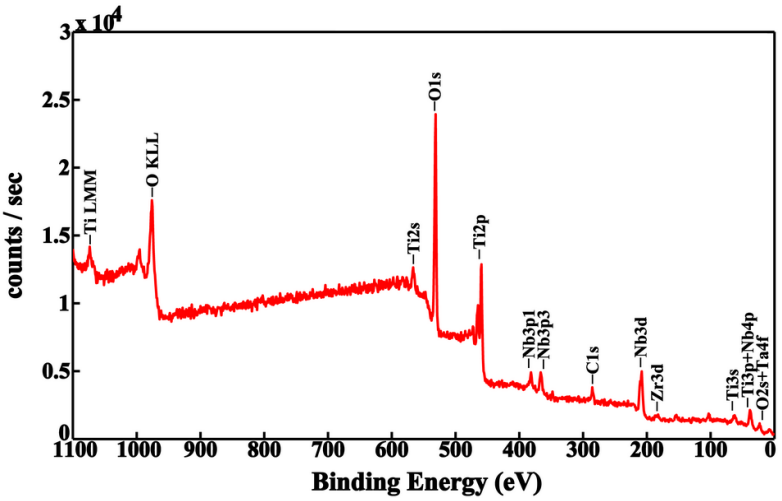

Figure 1. XPS survey spectrum of the initial surface of Ti-23Nb-0.7Ta-2Zr-1.2O alloy.

Taking into account the more complex composition and bigger thickness of the gum alloy native passive film, it results that this film is denser, more compact and thicker than that on Ti surface and is able to confer a better protection to the substrate.

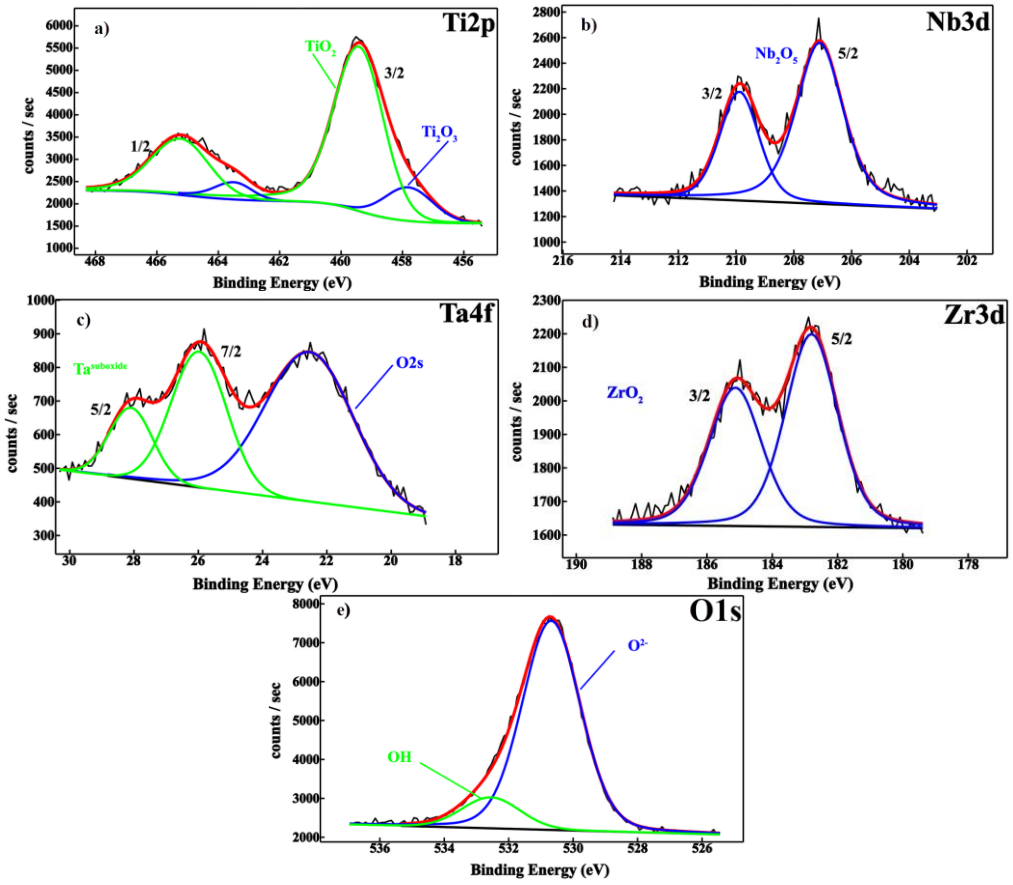

Figure 2. XPS deconvoluted spectra of the initial surface of Ti-23Nb-0.7Ta-2Zr-1.2O alloy: a) Ti 2p; b) Nd 3d; c) Ta 4f; d) Zr 3 d; e) O 1s.

3.2. Long-term electrochemical behavior of Ti-23Nb-0.7Ta-2Zr-1.2O alloy

The long-term electrochemical behavior of Ti23Nb-0.7Ta-2Zr-1.2O (gum) alloy was determined from voltammograms, Tafel representations, electrochemical impedance Nyquist and Bode spectra and from the monitoring of the open circuit potentials, E_{oc} and open circuit potential gradients, ΔE_{oc} for 2000 exposure hours in Ringer solutions of different pH values.

3.2.1. Long-term behavior from voltammograms and Tafel representations

Figure 3 presents the most important voltammograms for gum alloy at the initial time and after 1000 and 2000 immersion hours in Ringer solutions of acid (3.21), neutral (7.31) and alkaline (8.93) pH values. The curves reveal spontaneous passivity and large passive potentials ΔE_p domains characterized by the lower passive current densities, i_p which decreased over time, indicating more protective passive films, higher resistance to corrosion [8,29-33]; these passive films became more resistant in time due to the new depositions from the solutions which thickened the initial passive films.

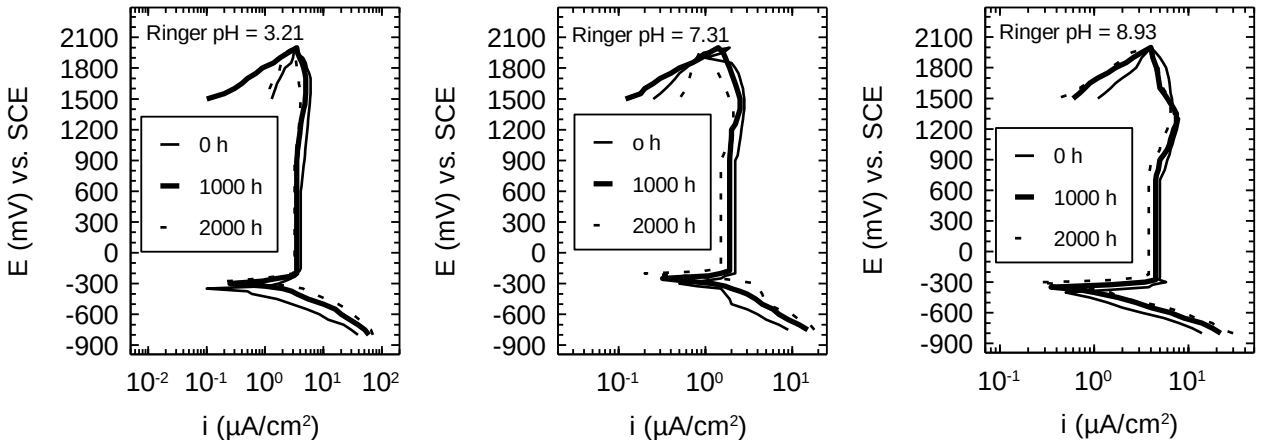

Figure 3. Voltammograms of Ti-23Nb-0.7Ta-2Zr-1.2O alloy in Ringer solutions of acid (3.21), neutral (7.31) and alkaline (8.93) pH values, for long-term exposure (1000 h and 2000 h), at 37^0C.

The new depositions were confirmed by the SEM micrographs (Fig. 4) obtained after 2000 immersion hours of gum alloy in Ringer solutions: in acid (pH = 3.21) Ringer solution (Fig. 4a), the depositions represent scattered particles with sub-micron size; in neutral (pH = 7.31) Ringer solution (Fig. 4b), denser particles can be observed which are responsible for the higher resistance to corrosion in time; in alkaline (pH = 8.93) Ringer solution (Fig. 4c), dense particles were also deposited. All particles had sub-micron dimensions; some pores appeared; thus, these new depositions enhanced the alloy native passive film increasing its protective properties and, in the same time, maintaining its porosity.

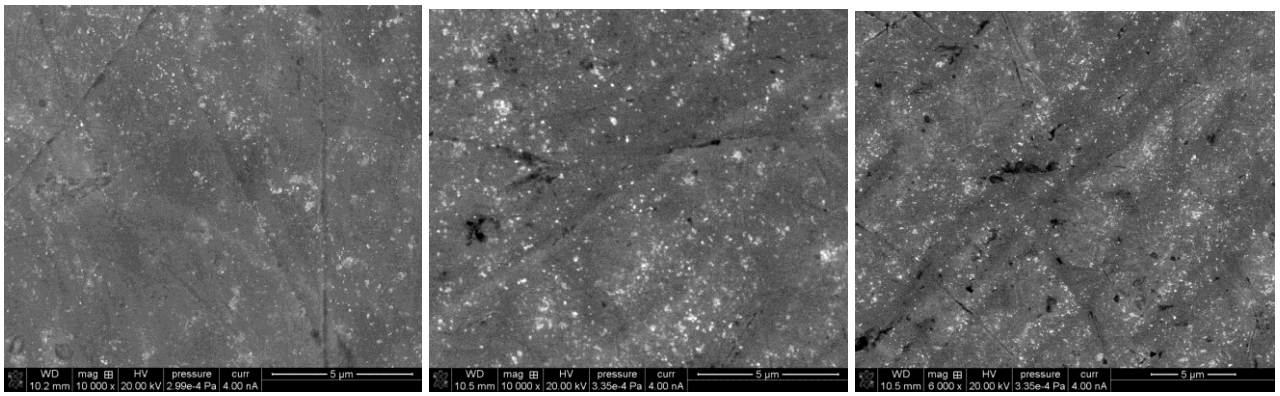

a) b) c)

Figure 4. SEM micrographs of Ti-23Nb-0.7Ta-2Zr-1.2O alloy surface after 2000 h in Ringer solutions of: a) pH = 3.21; b) pH = 7.31; c) pH = 8.93.

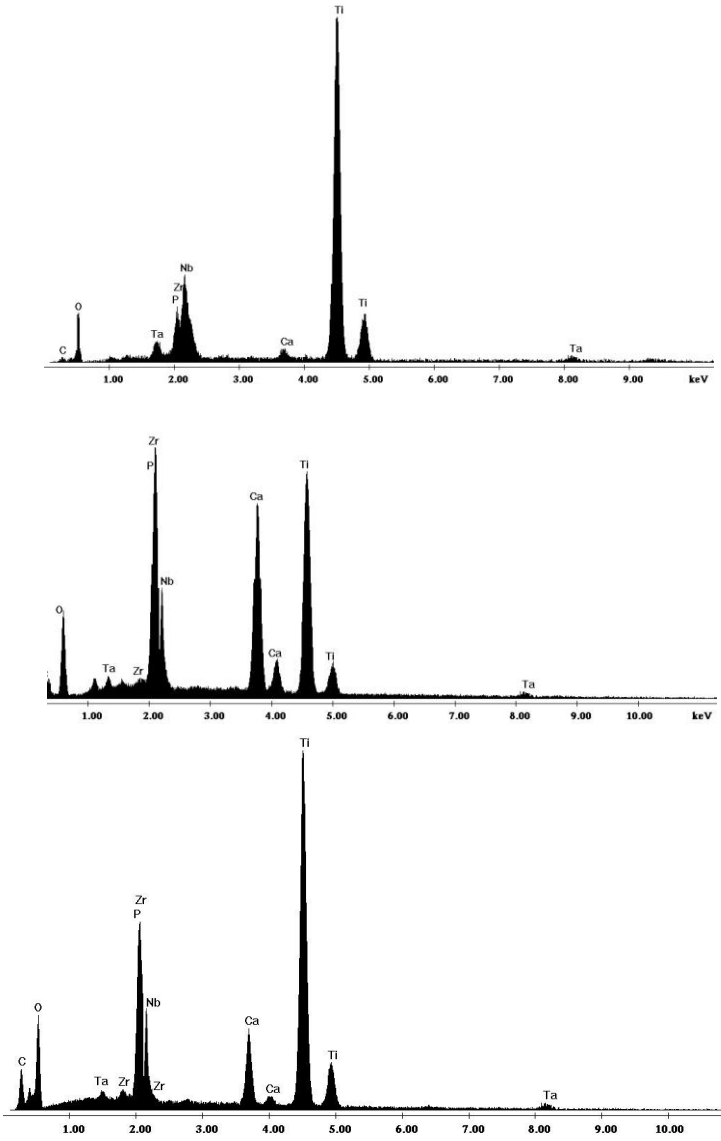

Figure 5. EDS spectra for Ti-23Nb-0.7Ta-2Zr-1.2O alloy surface after 2000 h in Ringer solutions of: a) pH = 3.21; b) pH = 7.31; c) pH = 8.93.

EDS elemental analysis (Fig. 5) attested the presence of calcium and phosphorous elements on the alloy surface, in higher quantity in neutral (Fig. 5b) and alkaline (Fig. 5c) Ringer solutions.

Very constant passive current densities can be observed (Fig. 3) for a large potential range, namely, the films progressively increased their thickness by the high field mechanism [34]. The corrosion potentials, E_{corr} slowly moved to positive direction, ennobled in time, fact that proves the improvement of the alloy passive properties. The increase of the passive current densities in the potential domain from +1.2 V till +1.7 V, was explained by some authors as being only oxidation processes into solution as oxygen evolving, oxidation of Ti^{3+} ions to Ti^{4+} ions [35,36] and no transpassive dissolution [33].

Comparing with Ti, from Table 1 it resulted the nobler behavior of the alloy, sustained by the more electropositive potentials, (corrosion potential, E_{corr} and passivation potential, E_p), lower values of the tendency to passivation, $|E_{corr}-E_p|$ and passive current densities, i_p.

From Tafel representations were obtained the main corrosion parameters: polarization resistance, R_p, corrosion current density, i_{corr}, corrosion rates, V_{corr}, and ion release rates (Table 1).

Table 1. Corrosion parameters for Ti and Ti-23Nb-0.7Ta-2Zr-1.2O (gum) alloy in Ringer solution of different pH values, at 37^0C.

Material	Time (h)	E_{corr} (mV)	E_p (mV)	$\|E_{corr}-E_p\|$ (mV)	i_p ($\mu A/cm^2$)	R_p ($k\Omega\ cm^2$)	i_{corr} ($\mu A/cm^2$)	V_{corr} (μm/year)	Ion release rate (ng/cm^2)
Ringer pH = 3.21									
Ti	0	-400	-300	100	7.1	12.4	0.247	2.10	213.36
	1000	-420	-300	120	7.8	15.5	0.374	3.18	335.81
	2000	-450	-350	100	8.2	11.9	0.571	4.85	492.76
Gum	0	-350	-250	100	4.1	19.2	0.202	1.85	193.76
	1000	-300	-200	100	3.5	20.2	0.186	1.58	160.63
	2000	-250	-200	50	3.2	23.5	0.154	1.31	132.99
Ringer pH = 7.31									
Ti	0	-320	-150	170	5.0	11.4	0.182	1.55	157.48
	1000	-350	-200	150	6.1	11.3	0.371	3.15	320.04
	2000	-380	-250	130	7.3	9.8	0.554	4.71	478.54
Gum	0	-250	-200	50	2.2	11.6	0.045	0.41	41.86
	1000	-230	-180	50	1.9	24.4	0.032	0.31	31.09
	2000	-220	-160	60	1.5	31.5	0.024	0.20	20.73
Ringer pH = 8.93									
Ti	0	-400	-200	200	10	13.9	0.321	2.78	182.45
	1000	-450	-300	150	11.4	11.5	0.417	3.54	359.66
	2000	-480	-350	130	12.5	9.8	0.593	5.04	512.06
Gum	0	-400	-300	100	5.0	16.9	0.215	1.83	185,72
	1000	-350	-300	50	4.5	21.4	0.201	1.71	173.63
	2000	-300	-250	50	3.8	25.3	0.185	1.57	159.82

Polarization resistances, R_p had higher values (order of tens $k\Omega\ cm^2$) in time, attesting higher resistance to corrosion. Values of i_{corr}, V_{corr} and the total quantity (ion release rate) of released ions (Table 1) were lower for gum alloy in comparison with Ti, as result of its denser passive layer that

contains both protective Ti oxides and very protective Nb, Zr, Ta oxides (XPS data) which assure structural integrity and enhance the alloy passive film, providing higher anticorrosion resistance [29,33,37,38].

Both electrochemical and corrosion parameters had the best values in neutral Ringer solution, where an implant "works" the most period from its "service lifetime".

3.2.2. Long-term behavior from EIS spectra

Nyquist spectra (Fig. 6) showed capacitive semicircles referring to the passive films [30,33,38,39]; semicircle diameters, impedance values increased over time, i.e., the oxide films thickened, became more compact developing better protection to the substrate. The inflexions from spectra are indicative for two layers [30,37].

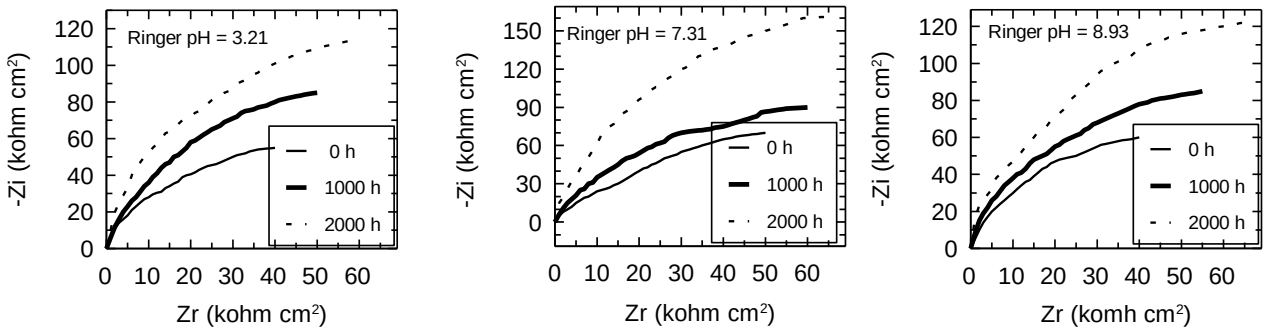

Figure 6. Nyquist spectra of Ti-23Nb-0.7Ta-2Zr-1.2O alloy in Ringer solutions of acid (3.21), neutral (7.31) and alkaline (8.93) pH values, for long-term exposure (1000 h and 2000 h), at 37^0C.

Bode phase angle spectra (Fig. 7) exhibited two peaks, two phase angles. The higher phase angle, in the low frequency range had values between $-78^0 \div -82^0$ in acid solution, between $-80^0 \div -85^0$ in neutral solution and between $-80^0 \div -82^0$ in alkaline solution. The high values of these phase angles certify very insulating passive films, [29-33,40], very protective inner layer like a barrier against the ion crossing through it. The lower phase angles, in the medium frequency range had values between $-74^0 \div -78^0$ in acid solution, between $-76^0 \div -80^0$ in neutral solution and between $-76^0 \div -79^0$ in alkaline solution. These lower values describe defective, lower insulating, less protective layer, outer layer which contains some pores where can take place some diffusion processes from the electrolyte. The values of the both high and low phase angles increased in time, being a supplementary argument for the improvement of the alloy protective capacity. Also, the most favorable phase angle values were registered in neutral Ringer solution, the normal functional condition of an implant alloy.

EIS spectra were modeled with two time constant equivalent electric circuit (Fig. 8) as many other authors [28, 41-44]: the first time constant, illustrated by R_1 resistance and CPE_1 capacitance, is associated with the barrier layer; the second constant, represented by R_2 resistance and CPE_2 capacitance, is related with the porous layer.

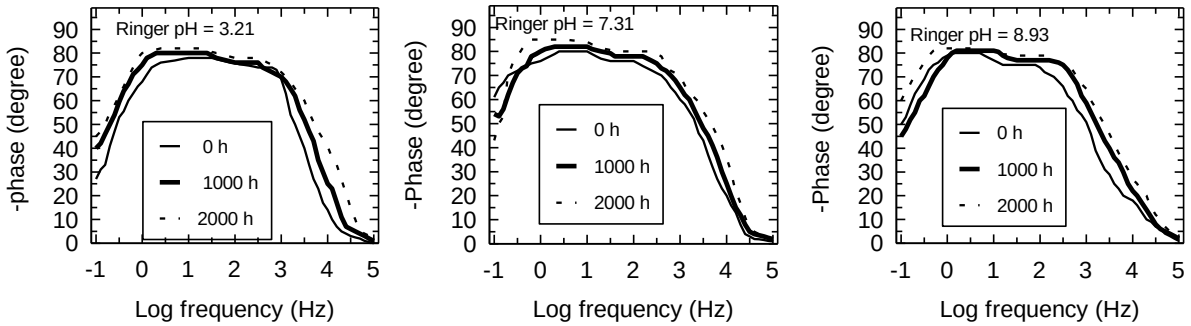

Figure 7. Bode phase angle spectra of Ti-23Nb-0.7Ta-2Zr-1.2O alloy in Ringer solutions of acid (3.21), neutral (7.31) and alkaline (8.93) pH values, for long-term exposure (1000 h and 2000 h), at 37^0C.

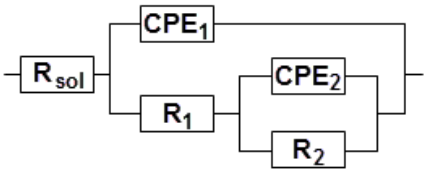

Figure 8. Electric equivalent circuit with two time constants fitted for the behavior of Ti-23Nb-0.7Ta-2Zr-1.2O alloy in Ringer solutions of acid (3.21), neutral (7.31) and alkaline (8.93) pH values, for long-term exposure (1000 h and 2000 h), at 37^0C.

The electrical parameters (Table 2) of the fitted electric equivalent circuit confirmed the insulating properties of the barrier layer by its very high resistance R_1 values (order of 10^6 Ω cm^2) and by the less protective properties of the porous layer by the resistance R_2 (order of 10^4 Ω cm^2); also, the values of the parameter n1, of near by one, prove an ideal capacitor for the barrier layer; the lower values of the parameter n2 indicate some interactions of the porous layer with the surrounding environment.

Table 2. Electrical parameters fitted for the electric equivalent circuit of Ti-23Nb-0.7Ta-2Zr-1.2O (gum) alloy in Ringer solutions of different pH values, at 37^0C.

Time (h)	R_{sol} (Ω cm^2)	R_1 (Ω cm^2)	CPE_1 (S S^n / cm^2)	n1	R_2 (Ω cm^2)	CPE_2 (S S^n / cm^2)	n2
Ringer pH = 3.21							
0	12.52	1.5 x 10^6	7.2 x 10^{-6}	0.90	0.43 x 10^4	5.4 x 10^{-5}	0.81
1000	13.01	3.2 x 10^6	5.5 x 10^{-6}	0.91	0.65 x 10^4	3.5 x 10^{-5}	0.82
2000	13.92	6.8 x 10^6	3.7 x 10^{-6}	0.94	0.86 x 10^4	1.7 x 10^{-5}	0.83
Ringer pH = 7.31							
0	13.23	3.7 x 10^6	6.8 x 10^{-6}	0.95	1.3 x 10^4	4.7 x 10^{-5}	0.82
1000	13.75	6.2 x 10^6	4.7 x 10^{-6}	0.97	1.9 x 10^4	2.8 x 10^{-5}	0.84
2000	14.21	8.5 x 10^6	2.9 x 10^{-6}	0.98	2.7 x 10^4	1.9 x 10^{-5}	0.85
Ringer pH = 8.93							
0	12.43	1.4 x 10^6	7.1 x 10^{-6}	0.91	0.4 x 10^4	5.3 x 10^{-5}	0.80
1000	13.18	3.3 x 10^6	5.3 x 10^{-6}	0.92	0.6 x 10^4	3.2 x 10^{-5}	0.81
2000	13.75	6.7 x 10^6	3.4 x 10^{-6}	0.93	0.9 x 10^4	1.9 x 10^{-5}	0.83

3.2.3. Long-term behavior from variations of the open circuit potentials and corresponding open circuit potential gradients

The open circuit potentials both for Ti and gum alloy (Fig. 9) ennobled during about 1000 immersion hours and subsequently reached about constant values for gum alloy and had some variations for Ti. This difference of behavior indicates the thickening of the alloy passive layer and some dissolution and repassivation processes for Ti [45,46] and can be explained by the very high anticorrosive resistance of the alloy passive film that contains both protective TiO_2 and very protective Nb_2O_5 and ZrO_2 (XPS data). For gum alloy, values of -240 mV in acid, -180 mV in neutral and -260 mV in alkaline Ringer solutions are placed on Pourbaix diagrams [47] in the passivity potential domain of Ti and alloying elements, that demonstrates stable passive state [45,46] for long-term.

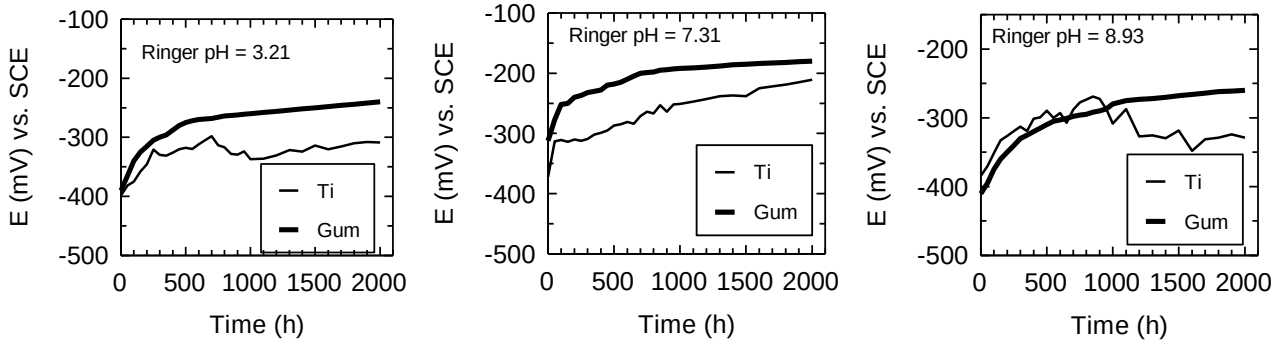

Figure 9. Time variations of the open circuit potentials for Ti and Ti-23Nb-0.7Ta-2Zr-1.2O alloy in Ringer solutions of acid (3.21), neutral (7.31) and alkaline (8.93) pH values, at 37^0C.

The open circuit potential gradients, ΔE_{oc} (Table 3) had very low values, proving that no galvanic or local corrosion can develop both on Ti and gum alloy surfaces in the case of the local variations of pH values along the implant surface [48-50].

Table 3. Open circuit potential gradients for Ti and Ti-23Nb-0.7Ta-2Zr-1.2O (gum) alloy in Ringer solutions at 37^0C.

Material	Time (h)	ΔE_{oc1} (mV)	ΔE_{oc2} (mV)	ΔE_{oc3} (mV)
Ti	0	-69.8	-66.7	+3.1
	1000	-89.8	-28.6	+61.2
	2000	-97.7	-20.4	+118.1
Gum alloy	0	-78.2	+20.3	+98.5
	1000	-68.5	+20.6	+88.3
	2000	-60.1	+20.7	+80.1

3.3. Macrophage cell response

The superior performance of an implantable material implies a good biocompatibility with the human body which depends on avoiding the adverse inflammatory reactions of the body to the

implant. Biomaterial chemistry might induce a complex cellular response at bone-implant interface that modifies the normal balance between bone formation and resorption resulting in osteolysis of the peri-prosthetic bone and finally in the aseptic loosening of the prosthesis [51]. Various cell types are involved in the successful osseointegration as well as in the pathogenesis of osteolysis including osteoblasts, macrophages, osteoclasts, fibroblasts, etc. Among these, macrophages are major components of the mononuclear phagocyte system and might be directly involved in bone resorption [52]. Evaluating the early response of this cell type toward biomaterials is an efficient tool for predicting the long-term bioactivity of an implant. Although biomaterials composition is known to have a critical role in implant performance, little work has been focused on the effects of chemical composition on inflammatory cells behavior. Sethi et al. [53] investigated the secretion profile of TNF-α and IL-6 induced by the surface chemistry of Co-Cr-Mo alloy as compared to Ti-6Al-4V. They detected a higher level of secreted TNF-α induced by Co-Cr-Mo, while IL-6 production was inhibited by this surface. Another study investigated the macrophage activation induced by two types of stainless steel (SS), namely 316L and nitrogenated SS (NSS). Exposure of macrophages to both surfaces lead to the production of low levels of TNF-α but higher IL-1β expression [54]. More recently, Hamlet and Ivanovski [55] reported lower levels of pro-inflammatory markers induced by Ti-6Al-4V as compared to commercially pure titanium surface.

In this work we have evaluated the *in vitro* response of RAW 264.7 macrophages to the novel composition of gum metal alloy (Ti-23Nb-0.7Ta-2Zr-1.2O) by examining cell viability and morphology as well as the temporal cytokine/chemokine expression profile. In order to investigate how biomaterial chemistry affects the viability and proliferation capacity of RAW 264.7 macrophages after 24 h and 48 h of maintenance on the test materials, MTT assay was undertaken (Fig. 10A). The absorbance levels indicated that the gum alloy surface is able to support the early adhesion and proliferation of RAW 264.7 cells both in standard and LPS-stimulated conditions in a similar manner with the reference material. No significant differences between the analyzed samples were remarked for both incubation periods. Notably, the number of metabolically active, viable cells increased during the culture time suggesting that these surfaces are suitable for cellular proliferation. The macrophage-like cell compatibility of gum metal might be a favorable aspect for wound healing process. Previous reports have also shown that enhanced initial macrophage accumulation was associated with improved wound healing [56,57]. Furthermore, the influence of material chemistry on macrophage morphological features plays an important role in determining the implant functionality. To evaluate the RAW 264.7 cells cytoskeleton organization we performed the immunofluorescent staining of actin after 24 h and 48 h of culture, in the presence or absence of LPS (Fig. 10B). The fluorescent visualization of cell morphology confirmed that RAW 264.7 macrophages adhered and proliferated on both titanium-based biomaterial surfaces. Cells attached to gum alloy or Ti surfaces in non-stimulated conditions exhibited a typical macrophage-like morphology displaying predominantly a round shape. Images corresponding to cells treated with LPS highlight enlarged macrophages with round morphology and, also, cells with a spindle-like shape and ruffled membrane. It has been proposed that a round shape is associated with resting, non-activated macrophages, while bigger and elongated cells indicate an activated macrophage phenotype [58]. Therefore, these results clearly suggest that, under

standard culture conditions, the chemical composition of gum alloy does not prime macrophages for activation and hence does not elicit a strong inflammatory reaction.

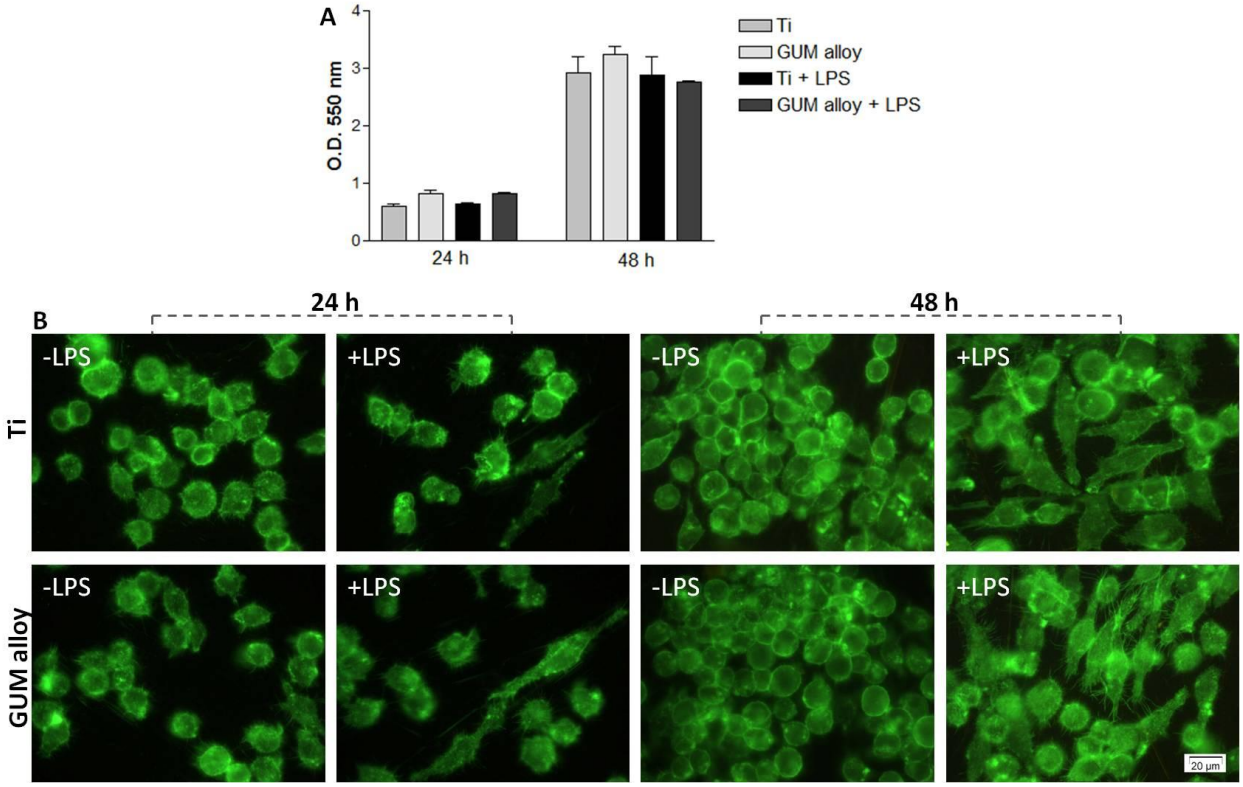

Figure 10. Viability/proliferation status (A) and morphology (B) of RAW 264.7 macrophages grown onto gum alloy *vs*. Ti at 24 h and 48 h, in the absence or presence of LPS. These cellular parameters were assessed by MTT test and Alexa-Fluor 488-phalloidin staining, respectively. Data analysis was based on mean ±SD (n=3). Scale bar = 20 µm.

The activation status of RAW 264.7 macrophages was further investigated by determining the protein concentration of pro-inflammatory TNF-α cytokine as well as MIP-1α and RANTES chemokines secreted in the culture medium by ELISA technique (Fig. 11). TNF-α is a cytokine associated with aseptic loosening, increasing the osteoclast survival rate and osteoclast maturation [59]. Moreover, it was shown that this cytokine is involved in inducing apoptosis of adherent macrophages on biomaterials [60]. MIP-1α and RANTES are reported to play an active role in monocytes chemotaxis and recruitment during inflammatory processes [61,62]. By measuring the surface-dependent response of macrophages in terms of cytokine/chemokine profile, our results show a significant increase in the production of all analyzed pro-inflammatory mediators by LPS-treated cells both at 24 h and 48 h post-seeding. No statistically significant differences were found between gum metal and Ti with respect to the secretion of TNF-α, MIP-1α and RANTES induced by the exposure of RAW 264.7 cells to titanium-based biomaterials, although smaller amounts were detected in the case of the gum metal alloy for all analyzed mediators. Most significantly, it was found that the expression levels of pro-inflammatory factors generally decreased with the culture time. This decrease from 24-h time point to 48-h time point was remarked especially upon stimulation with LPS, as follows: $p<0.001$

(gum alloy; Ti) for TNF-α; $p<0.01$ (Ti) for MIP-1α; $p<0.001$ (gum alloy; Ti) for RANTES. Therefore, the contact between macrophages and gum alloy or reference biomaterial did not support a persistent inflammatory response. Consequently, this study provides additional evidence that the gum alloy displays a biocompatible surface.

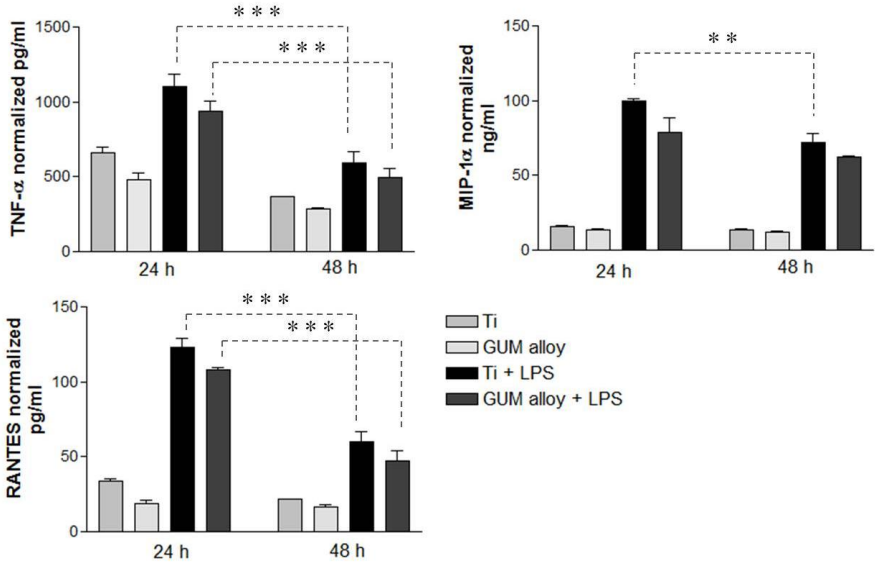

Figure 11. Temporal secretion profiles of TNF-α, MIP-1α and RANTES after 24 h and 48 h of culture of RAW 264.7 cells onto gum alloy and Ti under standard or LPS-stimulated conditions. Data analysis was based on mean ±SD (n=3). **p<0.01; ***p<0.001.

4. CONCLUSIONS

On gum metal alloy surface exists a native passive film consisting from very protective TiO_2, Nb_2O_5, ZrO_2 oxides and tantalum suboxides; this film has a thickness of about 6.5 nm ± 1 nm, is denser, more compact and thicker than that on Ti surface and is able to confer a better protection to the substrate.

Long-term behavior from voltammograms indicated more protective passive films, higher resistance to corrosion; these passive films became more resistant in time due to new depositions from the solutions which thickened the initial passive films. SEM micrographs confirmed new depositions formed by dense nanoparticles with some pores. EDS elemental analysis attested the presence of calcium and phosphorous elements on the alloy surface.

Corrosion parameters had more favorable values for Ti-23Nb-0.7Ta-2Zr-1.2O alloy than for Ti, as result of the alloy more protective passive film that assured the alloy structural integrity and anticorrosion resistance.

EIS spectra were modeled with two time constant equivalent electric circuit; the electrical parameters confirmed the insulating properties of the barrier layer and the less protective properties of

the porous layer. Some interactions of the porous layer with the surrounding environment took place over time.

In vitro studies regarding the behavior of RAW 264.7 macrophages demonstrated that the gum metal elicits a comparable biologic performance with Ti in terms of cell survival and proliferation, morphology and pro-inflammatory mediator secretion. These data together with the good biocompatibility with bone cells, already demonstrated, suggest that the gum metal alloy holds great promise for applications in orthopedics.

ACKNOWLEDGEMENTS
This work was supported by Romanian Ministry of National Education, CNCS-UEFISCDI (project PN-II-ID-20-RO-FR-2014) and by the French ANR (project ANR-13-IS09-0008-01)**.** Support of the EU (ERDF) and Romanian Government infrastructure POS-CCE O 2.2.1 project INFRANANOCHEM – No. 19/2009 is gratefully acknowledged.

References

1. M. Geetha, A.K. Singh, R. Asokamani and A.K. Gogia, *Prog. Mater. Sci*. 54 (2009) 397
2. R. Huiskes, H. Weinans and B. Vanrietbergen, *Clin. Orthop. Relat. Res*. 124 (1992) 124
3. M. Niinomi, *J. Mech. Behav. Biomed. Mater.* 1 (2008) 30
4. M. Niinomi, T. Hattori, K. Morikawa, T. Kasuga, A. Suzuki, H. Fukui and S. Niwa, *Mater. Trans.* 43 (2002) 2970
5. D.M. Gordin, T. Gloriant, G. Texier, I. Thibon, D. Ansel, J.L. Duval and M.D. Nagel, *J. Mater. Sci.: Mater. Med.* 15 (2004) 885
6. E. Bertrand, T. Gloriant, D.M. Gordin, E. Vasilescu, P. Drob, C. Vasilescu and S.I. Drob, *J. Mech. Behav. Biomed. Mater.* 3 (2010) 559
7. D. Kuroda, M. Niinomi, M. Morinaga, Y. Kato and T. Yashiro, *Mater. Sci. Eng. A* 243 (1998) 244
8. D. Mareci, R. Chelariu, D.M. Gordin, G. Ungureanu and T. Gloriant, *Acta Biomater*. 5 (2009) 3625
9. T. Saito, T. Furuta, J. Hwang, S. Kuramoto, K. Nishino, N. Suzuki, R. Chen R et al, *Science* 300 (2003) 464
10. R.J. Talling, R.J. Dashwood, M. Jackson and D. Dye, *Scripta Mater*. 60 (2009) 1000
11. M. Besse, P. Castany and T. Gloriant, *Acta Mater.* 59 (2011) 5982
12. E. Eisenbarth, D. Velten, M. Muller, R. Thull and J. Breme, *Biomaterials* 25 (2004) 5705
13. P. Thomsen, C. Larsson, L.E. Ericson, L. Senneby, J. Lausama and B. Kasemo, *J. Mater. Sci*. 8 (1997) 653
14. D.M. Gordin, R. Ion, C. Vasilescu, S.I. Drob, A. Cimpean and T. Gloriant, *Mater. Sci. Eng. C* 44 (2014) 362
15. M.A. Baker, S.I. Assis, R. Grilli and I. Costa, *Surf. Interface Anal*. 40 (2008) 220
16. R. Van Noort, *Biomaterials* 20 (1999) 3801
17. E. Vasilescu, P. Drob. D. Raducanu, I. Cinca, D. Mareci, J.M. Calderon Moreno, M. Popa, C. Vasilescu and J.C. Mirza Rosca, *Corros. Sci.* 51 (2009) 2885
18. A. Hynowska, E. Pellicer, J. Fornell, S. Gonzalez, N van Steenberge, S. Surinach, A. Gebert, M. Calin, J. Eckert, M.D. Baro and J. Sort, *Mater. Sci. Eng. C* 32 (2012) 2418
19. R. Huang and Y. Han, *Mater. Sci. Eng. C* 33 (2013) 2353
20. Y. Bai, Y.L. Hao, S.J. Li, Y.Q. Hao, R. Yang and F. Prima, *Mater. Sci. Eng. C* 33 (2013) 2159
21. J.M. Calderon Moreno, C. Vasilescu, S.I. Drob, S. Ivanescu, P. Osiceanu, P. Drob, M. Popa, S. Preda and E. Vasilescu, *J. Alloy Compd*. 612 (2014) 398

22. C. Vasilescu, S. I. Drob, E. I. Neacsu and J.C. Mirza Rosca, *Corros. Sci*. 65 (2012) 431
23. R. Ion, D.M. Gordin, V. Mitran, P. Osiceanu, S. Dinescu, T. Gloriant and A. Cimpean, *Mater. Sci. Eng. C* 35 (2013) 411
24. 24, P. Neacsu, D.M. Gordin, V. Mitran, T. Gloriant, M. Costache and A. Cimpean, *Mater. Sci. Eng. C* 47 (2015) 105
25. J.F. Moulder, W.F. Stickle, P.E. Sobol and K.D. Bomben, *Handbook of X-ray photoelectron spectroscopy,* Physical Electronics USA, Inc., Chanhassen (1995)
26. A.V. Naumkin, A. Kraut-Vass, S.W. Gaarenstroom and C.J. Powell, *NIST X-ray photoelectron spectroscopy database. NIST standard reference database 20, version 4.1.* US Secretary of Commerce on behalf of the United States of America (2012)
27. D.R. Baer, M.H. Egelhard, A.S. Lea, P. Nachimuthu, T.C. Droubay, J. Kim, B. Le, C. Mathews, R.L. Opila, L.V. Saraf, W.F. Stickle, R.M. Wallace and B.S. Wright, *J. Vac. Sci. Technol. A,* 28 (2010) 1060
28. M.T. Woldemedhin, D. Raabe and A.W. Hassel, *Electrochim. Acta* 82 (2012) 324
29. S.L. Assis, S. Wolynec and I. Costa, *Electrochim. Acta* 51 (2006) 1815
30. M. Khartega, V. Raman and N. Rajendran, *Acta Biomater*. 3 (2007) 1019
31. S.L. Assis and I. Costa, *Mater. Corros*. 58 (2007) 329
32. I. Cvijovic-Alagic, Z. Cvijovic, J. Bajat and M. Rakin, *Corros. Sci*. 83 (2014) 245
33. V.A. Alves, R.Q. Reis, I.C.B. Santos, D.G. Souza, T. de F. Goncalves, M.A. Pereira-da-Silva, A. Rossi and L.A. da Silva, *Corros. Sci*. 51 (2009) 2473
34. M.M. Lohrengel, *Mater. Sci. Eng. R* 11 (1993) 243
35. P.J. Boddy, *J. Electrochem. Soc.* 115 (1968) 199
36. C. Fonseca and A. Barbosa, *Corros. Sci*. 43 (2001) 547
37. I.C. Lavos-Valereto, S. Wolynec, I. Ramires, A.C. Guastaldi and I. Costa, *J. Mater. Sci.: Mater. Med.* 15 (2004) 55
38. W. Simka, M. Kaczmarek, A. Baron-Wiechec, G. Nawrat, J. Marciniak and J. Zak, *Electrochim. Acta* 55 (2010) 2437
39. A. Robin, O.A.S. Carvalho, S.G. Schneider and S. Schneider, *Mater. Corros*. 59 (2008) 929
40. S. Tamilselvi and N. Rajendran, *Mater. Corros*. 58 (2007) 285
41. S.L. Assis, S. Wolynec and I. Costa, *Mater. Corros*. 59 (2008) 739
42. S. Tamilselvi, V. Raman and N. Rajendran, *Electrochim. Acta* 52 (2006) 839
43. J. Pan, D. Thierry and C. Leygraf, *Electrochim. Acta* 41 (1996) 1143
44. F. Rosalbino, S. Desante, G. Borzone and G. Scavino, *J. Mater. Sci.: Mater. Med*. 23 (2012) 1129
45. J. Black, *Biological performance of materials: Fundamentals of biocompatibility*, M. Decker Inc. NY (1992)
46. D.J. Blackwood, A.W.C. Chua, K.H.W. Seah and R. Thampuran, *Corros. Sci*. 42 (2000) 481
47. M. Pourbaix, *Atlas of electrochemical equilibria in aqueous solutions,* NACE, Houston (1974)
48. E. Blasco-Tamarit, A. Igual-Munoz, J. Garcia Anton and D.M. Garcia-Garcia, *Corros. Sci*. 51 (2009) 1095
49. G. Sheela, M. Ramasamy, C.R.K. Rao and M. Pushpavanam, *Bull. Electrochem*. 17 (2001) 347
50. C. Sola, A. Amorim, A. Espias, S. Capelo, J. Fernandes, L. Proenca, L. Sanchez and I. Fonseca, *Int. J. Electrochem. Sci*. 8 (2013) 406
51. S.C. O'Neill, J.M. Queally, B.M. Devitt, P.P. Doran and J.M. O'Byrne, *Bone Joint J.* 95 (2013) 1022
52. M.H. Lee, D.W. Han, H.S. Baek, H.R. Lim, I.S.Lee, K.Y. Lee, K.T. Kim, S.J. Lee and J.C. Park, *Surf. Coat. Technol*. 201 (2007) 5729
53. R.K. Sethi, M.J. Neavyn, H.E. Rubash and A.S. Shanbhag, *Biomaterials* 24 (2003) 2561
54. S.S. Jakobsen, A. Larsen, M. Stoltenberg, J.M. Bruun and K. Soballe, *Eur. Cell Mater.* 14 (2007) 45
55. S. Hamlet and S. Ivanovski, *Acta Biomater*. 7 (2011) 2345

56. C. Robson, D.A. Dubay, X. Wang and M.G. Franz, *Wound Repair Regen.* 12 (2004) 38
57. X. Dai , Y. Wei, X. Zhang, S. Meng, X. Mo, X. Liu, X. Deng, L. Zhang and X. Deng, *J. Nanometer*. 2015 (2015) Article ID 712810
58. E. Saino, M.L. Focarete, C. Gualandi, E.Emanuele, A.I. Cornaglia, M. Imbriani and L. Visai, *Biomacromolecules* 12 (2011) 1900
59. C.C.G. Moura, D. Zanetta-Barbosa, P. Dechichi, V.F. Carvalho and P. B.F. Soares, *Braz. Dent. J.* 25 (2014) 96
60. W.G. Brodbeck M.S. Shive, E. Colton, N.P. Ziats and J.M. Anderson, *J. Lab. Clin. Med*. 139 (2002) 90
61. S. Chen, J.A. Jones, Y. Xu, H.Y. Low, J.M. Anderson and K.W. Leong, *Biomaterials* 31 (2010) 3479
62. D. Aldinucci and A. Colombatti, *Mediators Inflamm*. 2014 (2014) Article ID 292376